

Preparation of highly visible light active Fe–N co-doped mesoporous TiO₂ photocatalyst by fast sol–gel method

Kui Zhang · Xiangdong Wang · Xiaoling Guo ·
Tianou He · Yaming Feng

Received: 31 October 2013 / Accepted: 3 January 2014 / Published online: 14 January 2014
© Springer Science+Business Media Dordrecht 2014

Abstract A novel fast sol–gel method, using polyethylene glycol and polyacrylamide as bi-templates, to prepare the pure, Fe-doped, N-doped, and Fe–N co-doped mesoporous TiO₂ samples has been developed. The reaction time is reduced to a few hours for the present work. The IR spectrum has been used to investigate the reaction mechanism of the fast sol–gel method. The results indicate that the fast sol–gel process has been achieved due to the polymerization crosslink between hydrolysates of Ti alkoxides and templates by the intermolecular hydrogen bond. The prepared samples have been characterized by X-ray diffraction, transmission electron microscopy, X-ray photoelectron spectroscopy, N₂ adsorption–desorption, and UV–vis spectroscopy. The results show that the samples have a typical ordered mesoporous structure. The crystallite size, pore size, and surface area of Fe–N co-doped TiO₂ are about 13.6, 18.4 nm, and 172.08 m² g⁻¹, respectively. The iron species as the Fe³⁺ oxidation state are substitutionally doped into the TiO₂ lattice, and the doped nitrogen atom is incorporated into the TiO₂ lattice as the interstitial N. The co-doping of nitrogen and iron can enhance the absorption of visible region and inhibit

the recombination of photogenerated charge carriers, leading to higher photocatalytic activity for the co-doped sample than pure TiO₂ and solely doped with iron or nitrogen for degradation of methyl orange under visible light irradiation.

Keywords Mesoporous TiO₂ · Fast sol–gel · Fe–N co-doped · Photocatalysis

Introduction

Mesoporous TiO₂ has received much attention in recent years due to its chemical stability, nontoxicity, high absorptivity, and other excellent properties (Bian et al. 2011; Hartmann et al. 2010; Lee et al. 2008; Su et al. 2013). Although a variety of mesoporous TiO₂ materials have been fabricated for some applications in a wide range of areas such as dye-sensitized solar cells (Docampo et al. 2013; Huang et al. 2012), degradation of pollutant in water and air (Jing et al. 2005; Wang et al. 2012a, b), and hydrogen evolution (Chen et al. 2012; Silva et al. 2011), it remains a major challenge to prepare ordered mesoporous TiO₂ with high photocatalytic activity. There are many reports that mesoporous TiO₂ is prepared via various chemical methods such as hydrothermal synthesis, evaporation-induced self-assembly, precipitation reaction, and sol–gel process (Hung et al. 2010; Kumaresan et al. 2011; Wang et al. 2011; Yu et al. 2009). Among them, the sol–gel process is an attractive method, because it usually proceeds at room temperature and has some advantages, such as the

K. Zhang · X. Wang (✉) · T. He
School of Science, Xi'an Jiaotong University,
Xi'an 710049, China
e-mail: wang90xd@163.com

X. Guo · Y. Feng
School of Textile and Materials, Xi'an Polytechnic
University, Xi'an 710048, China

product obtained is highly pure, all reactants can homogeneously react with molecular form, which is in favor of doping process, and mesoporous TiO₂ materials prepared have a wide variety of morphologies by adjusting the conditions in the process. However, there are two distinct problems for preparing mesoporous TiO₂ by the conventional sol–gel method. Firstly, it takes too much time in the synthetic process. The gelation time usually lasts a week or more. Secondly, the block polymer, the template usually for preparing the mesoporous TiO₂, is an expensive material, which limits the application of the sol–gel method (Blondeau and Coradin 2012; Choi et al. 2007; Wang et al. 2010). Zhang et al. (2010) prepared mesoporous TiO₂ by a conventional sol–gel process, in which titanium isopropoxide was used as a precursor and triblock copolymer Pluronic P123, F108, and F127 were used as the templates, the gelation time needs 5 days, and the whole process lasts more than a week. Therefore, it is urgent to develop a modified sol–gel method for accelerating sol–gel process and search for inexpensive templates.

Furthermore, in order to utilize the solar energy effectively, many studies on the modification of TiO₂ doped with metals and nonmetals have been carried out to extend the absorption band edge of TiO₂ into the visible region. Especially nitrogen doping (Ananpattarachai et al. 2009; Asahi et al. 2001; Halasi et al. 2012; Liu et al. 2012), which can create a mid-gap state acting as an electron donor or acceptor in the band gap of TiO₂, effectively enhances visible light photocatalytic activity of the material. On the other hand, the photocatalytic reaction efficiency depends on the competition between the surface charge carrier transfer rate and the electron–hole recombination rate. It is found that Fe³⁺ doped can enhance photocatalytic activity, which is because small amount of Fe³⁺ ions can act as traps of the photo-generated electrons and holes, and inhibit the electron–hole recombination (Goswami and Ganguli 2012; Li et al. 2010; Yu et al. 2012; Zhou et al. 2005). Furthermore, the majority of research reports exhibited that iron and nitrogen are incorporated into TiO₂ together to narrow the band gap more effectively and promote the separation of the photogenerated electrons and holes to accelerate the transmission of photocurrent carrier, enhancing the photocatalysis of co-doped TiO₂ under visible light (Cong et al. 2007; Hao and Zhang 2009; Mangham et al. 2011; Rane et al. 2006; Zhou et al. 2005).

In the present paper, we have developed a facile fast sol–gel method, in which the costless polyacrylamide (PAM) and polyethylene glycol (PEG) were used as the

bi-templates. The pure TiO₂, N-doped TiO₂ (N–TiO₂), Fe-doped TiO₂ (Fe–TiO₂), and Fe–N co-doped TiO₂ (Fe–N–TiO₂) photocatalysts with ordered mesoporous structure were prepared. The reaction time was reduced from about 1 week to several hours. The reaction mechanism of the fast sol–gel method has been studied. The photocatalytic activities of the photocatalysts were evaluated by measuring the photocatalytic degradation of methyl orange (MO) in water under visible light irradiation. Fe–TiO₂, N–TiO₂, and Fe–N co-doped TiO₂ exhibit higher photocatalytic activity than pure TiO₂ under visible light irradiation, due to the doping that has decreased the band gap and promoted the separation of the photogenerated electrons and holes. It also has been proved that the photocatalytic activities of mesoporous nanoparticles are stable and durable by the cycle photocatalytic test.

Experimental

Preparation of photocatalysts

The Fe–N–TiO₂ photocatalyst was fabricated by a fast sol–gel method. A total of 10 mL tetrabutyl titanate, 1.4 g urea, 1 g ferric nitrate, 5 mL nitric acid (5 wt%), and 10 mL deionized water were dissolved in 200 mL anhydrous ethanol, and the mixture was stirred for 0.5 h, the resulting solution was named solution A. A total of 0.02 g PAM (MW = 3,000,000 g mol⁻¹) and 0.8 g PEG (MW = 20,000 g mol⁻¹) were dissolved in 30 mL deionized water under vigorously stirring, named solution B. The solution B was slowly added to the solution A with vigorously stirring until the solution became transparent. After about 0.5 h, a white gel was formed, which was dried at 60 °C for 6 h. The gel was calcined in air at 450 °C for 4 h to obtain the photocatalyst. For comparison, pure mesoporous TiO₂, N–TiO₂, and Fe–TiO₂ were prepared according to the above procedure with the corresponding doped agent.

Characterizations

The IR spectrum (SENSOR27, Bruker, Germany) was used to study the reaction mechanism of the fast sol–gel method. The X-ray diffraction (XRD) patterns of photocatalysts were determined by XRD (Bruker D8 Germany) using Cu K α radiation and a step size of 0.02° in the range of 20°–80°. X-ray photoelectron

spectroscopy (XPS) analysis was obtained using a PHI 5300 ESCA instrument with an Mg $K\alpha$ X-ray source at a power of 250 W. The binding energy scale was calibrated with respect to the C1s peak of hydrocarbon contamination fixed at 284.6 eV. The morphology was examined by transmission electron microscopy (TEM) (JEM-2100F, Japan). N_2 adsorption isotherms were collected on a nitrogen adsorption apparatus (ASAP 2020 Micromeritics USA) at -196 °C, and all samples were degassed at 120 °C for 2 h. The UV–vis spectra were performed with a UV–vis spectrophotometer (U-4100, HITACHI, Japan). $BaSO_4$ was the reference sample, and the spectra were recorded at room temperature in air within the range 200–800 nm.

Evaluation of photocatalytic activity

Photocatalytic activity of the photocatalysts was evaluated by measuring the degradation of MO in water. The photocatalyst (0.05 g) was added into 70 mL of MO solution (10 mg L^{-1}), stirring for 30 min to equilibrate in the dark, and then irradiated by a 300 W xenon lamp through a UV-cutoff filter ($\leq 400 \text{ nm}$) used as the visible light source. The photocatalytic degradation was conducted in a BL-GHX-V multifunctional photochemical reactor. The analytic suspension (5 mL) was taken out of the reactor at regular intervals (every 1 h), which would be centrifuged immediately and then filtered with a membrane filter ($0.1 \mu\text{m}$) to separate TiO_2 from the solution. The residual concentration of MO solution was measured at 464 nm using a UV spectrometer (LAMBDA-950). The change of relative absorbance was used to record the change of concentration of MO in the solution, that is $C_t/C_0 = A_t/A_0$ (C_t , A_t referred to the concentration and absorbance of MO in the solution at time and C_0 , A_0 referred to the concentration and absorbance of MO in the solution at the initial time, respectively). As a comparison, the MO solution without any photocatalysts was also measured according to the above procedures.

Results and discussion

The reaction mechanism of the fast sol–gel method

The IR spectra of PEG, PAM, the dry gel of Fe–N co-doped TiO_2 (Fe–N– TiO_2 /PAM–PEG), and Fe–N co-

doped TiO_2 samples were performed to study the reaction mechanism of the fast sol–gel method as shown in Fig. 1. It can be seen that it is easy to identify PEG and PAM by their characteristic peaks in the Fig. 1a, b. According to the literature (Liu et al. 2010; Rahim et al. 2012), the peaks at $3,204.1 \text{ cm}^{-1}$ (ν_{O-H}), 2,920.3 and $1,383.1 \text{ cm}^{-1}$ (ν_{C-H}), and 1,626.6 and $1,121.3 \text{ cm}^{-1}$ (ν_{C-O}) are the characteristic peaks of PEG. The characteristic peaks of PAM are distributed at $3,426.4 \text{ cm}^{-1}$ (ν_{N-H}), $2,934.5 \text{ cm}^{-1}$ (ν_{C-H}), and 1,650.1 and $1,073.6 \text{ cm}^{-1}$ (ν_{C-O}). The absorption peak at $3,300\text{--}3,500 \text{ cm}^{-1}$ (Fig. 1c) for Fe–N– TiO_2 /PAM–PEG has become broad evidently. There are two reasons for this change. One is due to the overlap of the peaks of Ti–OH produced by hydrolysis of tetrabutyl titanate, the –OH of the PEG, and the –NH of the PAM. The other is intermolecular hydrogen bonds formed in the Ti–OH, PEG, and the acylamino of PAM (Gao and Bai 2013; Wang et al. 2007). The intermolecular hydrogen bond has also testified by contrasting the –C–O characteristic peak of PEG, PAM, and Fe–N– TiO_2 /PAM–PEG in the Fig. 1. Compared with the Fig. 1a and b, it can be found that the –C–O characteristic absorption peaks at 1,626.6 and $1,650.1 \text{ cm}^{-1}$ for PEG and PAM, respectively, were converted into $1,554.1$ and $1,621.2 \text{ cm}^{-1}$ for the Fe–N– TiO_2 /PAM–PEG (Fig. 1c). Additionally, the broad peak at 823.4 cm^{-1} (ν_{Ti-O}), originating from the TiO_2 , appears in the Fig. 1c and d and also indicates that PAM and PEG combine with TiO_2 by hydrogen bond in the Fe–N– TiO_2 /PAM–PEG (Gao and Bai 2013; Wang et al. 2007).

Figure 2 shows an illustration for the synthesis mechanisms of photocatalysts. In the present work, the Fe–N– TiO_2 was prepared by two steps. Firstly, fast

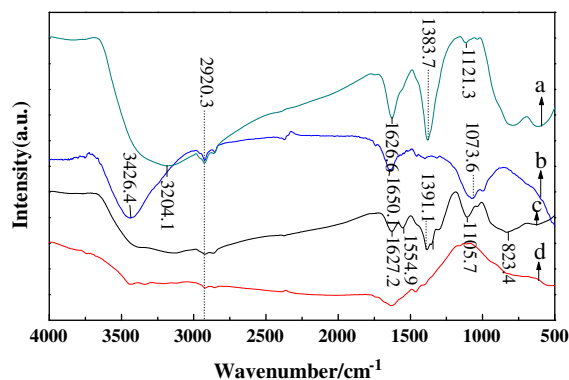


Fig. 1 IR spectra of a PEG; b PAM; c Fe–N– TiO_2 /PAM–PEG; d Fe–N– TiO_2 after calcined at 450 °C for 4 h

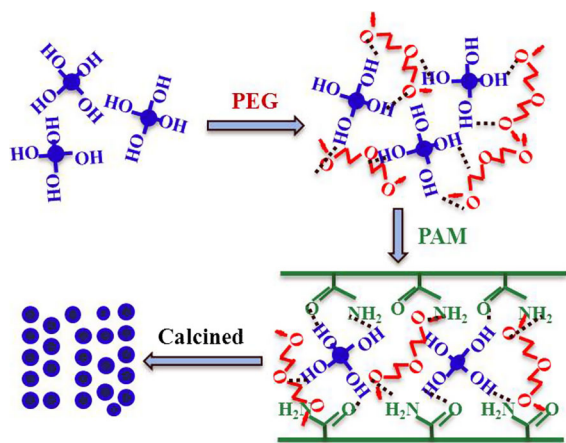


Fig. 2 An illustration for the synthesis mechanism of photocatalysts

sol-gel process was conducted using tetrabutyl titanate as the Ti source, urea as the N source, ferric nitrate as the Fe source, and PAM and PEG as the bi-temple. Due to its strong hydrophilicity, PEG can readily combine with titania sol produced from the hydrolyzation of tetrabutyl titanate to form the composite grains (Zhang et al. 2003; Zhou et al. 2012). The grains can incorporate with PAM by hydrogen bonding, and the grains are confined in the molecule networks of PAM. The hydrogen bonds lead to the polymerization crosslink between hydrolysates of tetrabutyl titanate and templates (Gao and Bai 2013; Liu et al. 2010; Wang et al. 2007; Zhang et al. 2003; Zhou et al. 2012). This crosslink is the primary cause that accelerates the sol-gel reaction velocity effectively. Secondly, the precursors prepared by a sol-gel process were calcined at air atmosphere. The PEG and PAM were decomposed successively on heating, and the Fe-N-TiO₂ with the order mesoporous structure and high surface area was obtained.

The analysis of photocatalyst

Figure 3a shows the XRD patterns of pure TiO₂, N-TiO₂, Fe-TiO₂, and Fe-N-TiO₂. Based on XRD data, the corresponding crystallite sizes were estimated using the Scherrer formula. The results were shown in Table 1. It is found that pure anatase phase was obtained using the fast sol-gel method and no other phases (brookite or rutile) were detected in all the samples. The results also revealed doping and co-

doping can retard crystal growth, due to the different radii of N, Fe, Ti, and O (Huang et al. 2013). Table 1 summarizes the surface area ($S_{\text{BET}}/\text{m}^2 \text{g}^{-1}$), pore diameter (d_p), and pore volume (V_p) of different photocatalysts calculated by the BJH method based on the nitrogen adsorption-desorption isotherms (Fig. 3b). The adsorption-desorption isotherms are consistent with type IV of hysteresis loops, which suggest uniform mesopores with a small size, similar to those observed in the previous report (Bian et al. 2011; Su et al. 2013), and the uniform pores with diameters ranging from about 16.5 to 18.5 nm further confirm that the mesoporous nanoparticles were prepared by the fast sol-gel method. The doped mesoporous nanoparticles exhibit higher S_{BET} values than pure mesoporous TiO₂, which could be attributed to both the increase in V_p and the decrease in crystallite sizes of the doped nanoparticles.

TEM and HRTEM images were used to further study the crystalline structure of Fe-N-TiO₂. It is found that ordered wormhole-like mesostructured TiO₂ nanoparticles were obtained by the fast sol-gel method (Fig. 4a). It can be estimated that the crystallite size distribution ranged from about 15 to 20 nm, which is in agreement with the XRD results. The images demonstrated that TiO₂ nanoparticles are not agglomerated and quite uniform in size and shape, indicating a typical of ordered mesoporous structure. The pore size is about 18.4 nm, which is consistent with N₂ sorption analysis. The HRTEM image (Fig. 4b) and the Debye rings (inset in Fig. 4b) confirm the polycrystalline structure of the nanocrystal. The average interplanar space of the nanocrystals is determined to be 0.351 nm, corresponding with (101) crystal facets of anatase TiO₂ (Huang et al. 2013).

The XPS analysis was performed in order to determine the chemical composition of the Fe-N-TiO₂ sample and identify the chemical state of Fe and N elements in the sample. Figure 5a, b shows the XPS survey spectra of the pure TiO₂ and Fe-N-TiO₂ samples. It can be found from Fig. 5b that, compared with the XPS survey spectra of the pure TiO₂, the peaks of titanium, oxygen, and carbon are evident. The weak peaks of nitrogen and iron can also be detected in the Fig. 5b. The binding energies of Ti2p, O1s, N1s, Fe2p, and C1s are 459.0, 531, 400.5, 710.5, and 284.6 eV, respectively, which are approximately in agreement with the previous data by other researchers

Fig. 3 **a** XRD patterns and **b** N₂ adsorption–desorption isotherms of pure TiO₂, N–TiO₂, Fe–TiO₂ and Fe–N–TiO₂

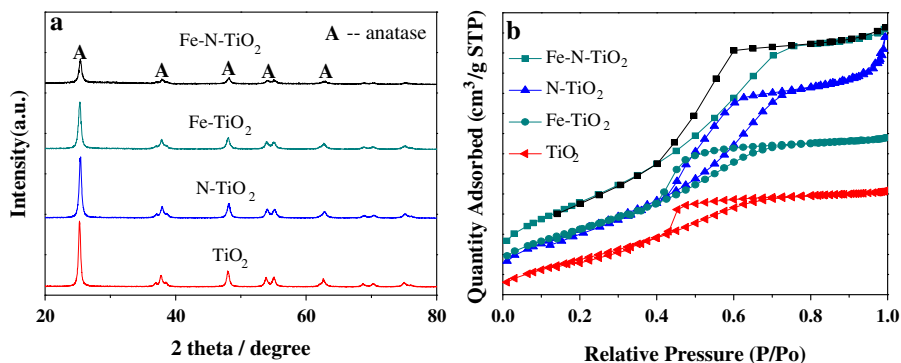


Table 1 The characterization results of different samples

Sample	Crystallite size/nm	S _{BET} /m ² g ⁻¹	Pore volume (V _p)/cm ³ g ⁻¹	Pore size (d _p)/nm
TiO ₂	15.4	154.37	0.09	16.85
Fe–TiO ₂	14.7	155.72	0.10	17.49
N–TiO ₂	14.1	162.99	0.12	17.93
Fe–N–TiO ₂	13.6	172.08	0.19	18.36

(Hao and Zhang 2009; Mangham et al. 2011; Rane et al. 2006; Xing et al. 2010). The C1s peak (284.6 eV) is usually associated with the residual carbon from precursor solution and the adventitious hydrocarbon from XPS instrument itself. The relative atomic concentrations of iron and nitrogen in the sample, especially that of the N atoms is low, estimated from the XPS data, were determined to be about 0.11 and 0.78 atom %, respectively.

Figure 5c shows the high-resolution XPS spectra of N1s region. Three XPS peaks at 399.1, 400.5, and 401.5 eV were observed. According to the literature (Asahi et al. 2001; Choi et al. 2007), the N1s peak at 400.5 eV can be attributed to the presence of oxidized N such as the structure of Ti–O–N in the TiO₂ lattice. The peak at 401.5 eV may be attributed to the bond of Ti–N–O (Asahi et al. 2001; Halasi et al. 2012; Huang et al. 2013; Liu et al. 2012). It is known that peak around 400 eV is related to oxidized nitrogen such as Ti–O–N or Ti–N–O binding (Asahi et al. 2001; Huang et al. 2013), so the peaks at 399.1 and 400.5 eV can be attributed to the anionic N⁻ in the interstitial N form (Halasi et al. 2012; Huang et al. 2013; Xing et al. 2010; Yang et al. 2010). It is found from Fig. 5c that the peak

at 400.5 eV has higher intensity than those of the peaks at 399.1 eV. Considering the XPS results above, in the present study, it is concluded that the interstitial N is the main form of doped nitrogen element incorporated into the TiO₂ lattice.

The high-resolution XPS spectra for Fe2p are shown in Fig. 5d. Two characteristic peaks, ascribed to Fe2p_{3/2} at 710.5 eV and Fe2p_{1/2} at 723.7 eV, appeared for the Fe–N–TiO₂ sample, indicating that the iron species as the Fe³⁺ oxidation state are substitutionally doped into the TiO₂ lattice (Goswami and Ganguli 2012; Hao and Zhang 2009; Mangham et al. 2011; Yang et al. 2010; Zhou et al. 2005). There is no evidence of Fe²⁺ in the sample. Since the radius of Fe³⁺ is similar to that of Ti⁴⁺, the Fe³⁺ could be incorporated into the lattice of TiO₂ to form Ti–O–Fe bonds in the Fe–N–TiO₂ sample. Furthermore, in the present work, the Fe–N–TiO₂ sample was prepared at the air atmosphere, the oxygen-rich condition, which is beneficial to the formation of the Fe³⁺ oxidation state (Hao and Zhang 2009; Mangham et al. 2011; Zhou et al. 2005). Thus, the Fe element in the sample exists mainly in the Fe³⁺ oxidation state.

The UV–vis diffuse reflectance spectra of the as-prepared photocatalysts are shown in Fig. 6. The light absorption of TiO₂ decreases sharply with the increased wavelength. Pure TiO₂ shows an intrinsic absorption with the light wavelength shorter than 390 nm, and there is almost no absorption in visible light with wavelength ranging from 400 to 800 nm. For doped TiO₂ nanoparticles, however, absorption intensity increases significantly in visible light region. The shift in the absorption band edges of the doped TiO₂ samples indicates that the optical band gap decreases in the order of Fe–TiO₂, N–TiO₂, and Fe–N–TiO₂. According to Asahi's method (Asahi et al. 2001), the band gap energies of Fe–TiO₂, N–TiO₂, and

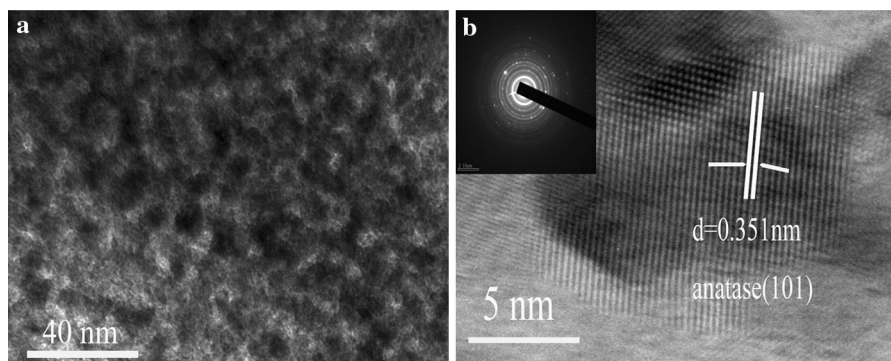
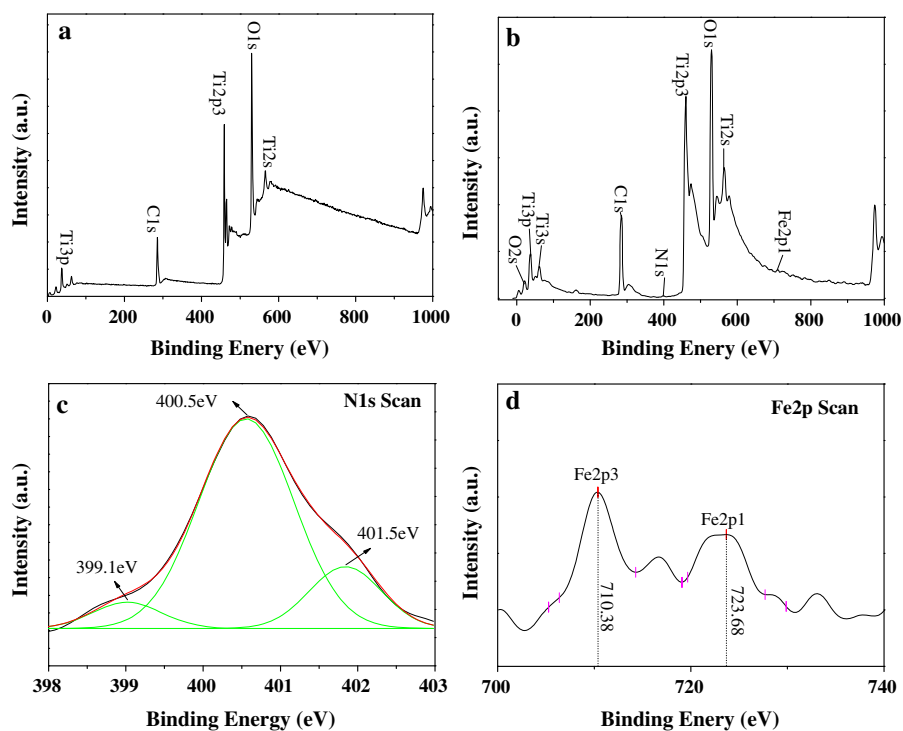


Fig. 4 **a** TEM and **b** HRTEM images of Fe–N–TiO₂

Fig. 5 **a, b** XPS survey spectra of pure TiO₂ and Fe–N–TiO₂, **c** high-resolution XPS spectra of N1s, **d** high-resolution XPS spectra of Fe2p



Fe–N-doped TiO₂ are estimated to be about 2.86, 2.71, and 2.56 eV, respectively, which are suitable for photocatalytic degradation of organic pollutants under visible light irradiation, while band gap energy of pure TiO₂ is 3.18 eV. The enhanced light absorption in the visible range and band gap narrowing of doped TiO₂ are attributed to N or Fe, and Fe–N co-doping, which can induce the local states above the valence band edge (Hao and Zhang 2009; Mangham et al. 2011; Spadavecchia et al. 2012).

Photocatalytic activity

The visible photocatalytic activity of doped TiO₂ samples was evaluated by measuring the decomposition of MO solutions under visible light irradiation at room temperature. The photocatalytic behavior of pure TiO₂ was also measured as a comparison. Figure 7a shows the concentration change of MO for different samples against the reaction time. A blank test indicates that in the absence of photocatalysts,

decoloration of the MO solution is negligible during the tested period. Compared with the pure mesoporous TiO₂, doped TiO₂ samples have higher photocatalytic activity, especially for the Fe–N co-doped TiO₂. The overall degradation rate of MO for Fe–N–TiO₂, N–TiO₂, Fe–TiO₂, and pure TiO₂ after 8 h of irradiation are 67, 61, 54, and 11 %, respectively. From kinetic studies on photocatalytic reactions of samples, as the literature reported, the degradation reaction can be well explained by a pseudo-first-order pattern (Ananpattarachai et al. 2009; Hu et al. 2010; Wu et al. 2011; Zhou et al. 2013). Figure 7b shows the slope of the graph plotted between ln(C₀/C) and the reaction time. Results show that under visible light irradiation for 8 h, the degradation rate contents of MO are 12.9,

12.1, 9.9, and 0.7 (×10⁻² h⁻¹) for Fe–N–TiO₂, N–TiO₂, Fe–TiO₂, and pure TiO₂, respectively.

The above difference of photocatalytic activity can be attributed to Fe, N, and Fe–N co-doping. The incorporation of Fe and N elements into the TiO₂ results in an evident red-shift of the absorption of TiO₂, because a new energy band is formed between the conduction band and the energy band in the mesoporous Fe–N–TiO₂ sample (Mangham et al. 2011; Yang et al. 2010). Another important factor is doped Fe³⁺ ions, which have a half-filled stable electronic configuration (d⁵). When Fe³⁺ ions trap electrons, they form less stable Fe²⁺ ions. The trapped electrons can easily be transferred to the oxygen adsorbed on the surface of the sample, and Fe²⁺ ions change into the original stable Fe³⁺ ions. Thus, photoexcited electrons and holes are effectively separated, enhancing the photocatalytic activity (Hao and Zhang 2009; Mangham et al. 2011; Wu and Krol 2012; Zhou et al. 2005). The photocatalytic activity of the pure mesoporous TiO₂ and doped TiO₂ samples is in agreement with their test results of the UV–Vis diffuse reflectance spectra.

To confirm their stability and durability for the decomposition of MO, the three cyclic photocatalytic degradation tests of MO aqueous solution were carried out for the Fe–N–TiO₂, N–TiO₂, and Fe–TiO₂ samples under visible light irradiation. It is found that after three recycling degradation tests, the photocatalysts can still degrade MO and the degradation rates of each cycling remain almost the same within 8.5 h, as shown in Fig. 8, suggesting their good cyclic usage and high stability. The results indicate that cyclic usage of the

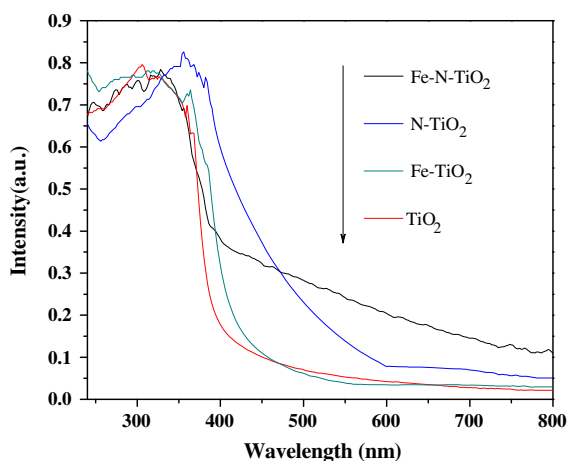


Fig. 6 UV–vis diffuse reflection spectra of pure TiO₂, Fe–TiO₂, N–TiO₂, and Fe–N–TiO₂ samples

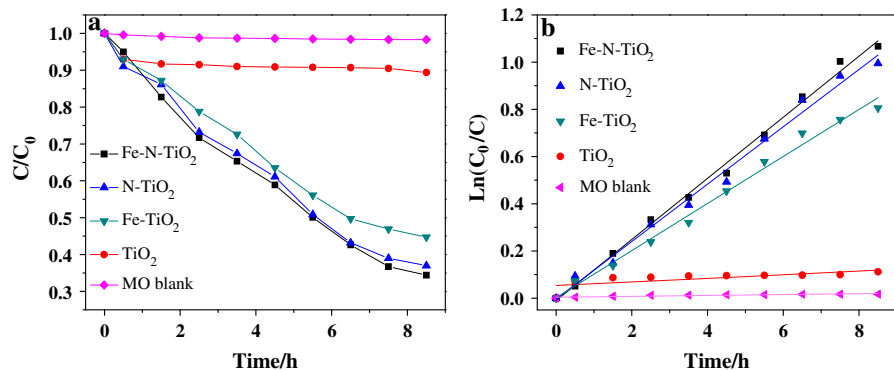


Fig. 7 Photocatalytic degradation of MO solutions using pure TiO₂, Fe–TiO₂, N–TiO₂, and Fe–N–TiO₂ samples under visible light irradiation: **a** C/C₀ ~ t and **b** ln(C₀/C) ~ t

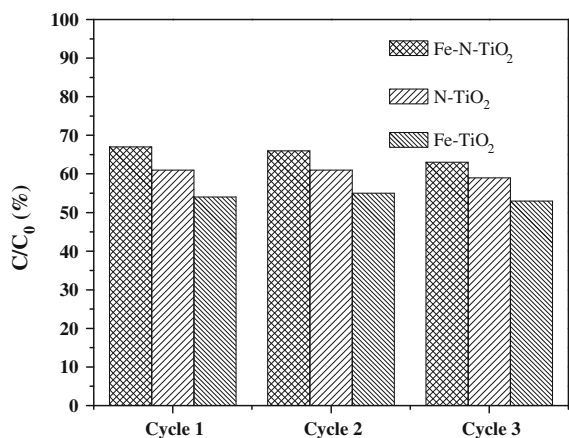


Fig. 8 Photocatalytic degradation of MO solutions using Fe-TiO₂, N-TiO₂, and Fe-N-TiO₂ samples for three cyclic uses

samples is possible and these materials have a good stability and durability for practical applications.

Conclusions

In summary, Fe-N co-doped mesoporous TiO₂ photocatalyst with high surface area, well-order mesoporous structure, and high visible light photocatalytic activity was successfully prepared via the fast sol-gel method by introducing PAM and PEG as the bi-templates. The sol-gel reaction velocity is accelerated evidently, and reaction time is reduced to several hours. This could be attributed to the polymerization crosslink of the hydrolysates of Ti alkoxides and templates produced by the intermolecular hydrogen bond. The fast sol-gel method may have more potential for practical application than the conventional sol-gel method, because of its fast preparation process and lower cost for templates.

Acknowledgments This work was supported by the Science and Technology Planning Project of Shaanxi Province (2013K09-04) and the Scientific Research Project of the Provincial College Key Laboratory of Shaanxi Province (2010JS007).

References

Ananpattarachai J, Kajitvichyanukul P, Seraphin S (2009) Visible light absorption ability and photocatalytic oxidation activity of various interstitial N-doped TiO₂ prepared from different nitrogen dopants. *J Hazard Mater* 168:253–261. doi:10.1016/j.jhazmat.2009.02.036

Asahi R, Morikawa T, Ohwaki T, Aoki K, Taga Y (2001) Visible-light photocatalysis in nitrogen-doped titanium oxides. *Science* 293:269–271. doi:10.1126/science.1061051

Bian Z, Zhu J, Wen J, Cao F, Huo Y, Qian X, Cao Y, Shen M, Li H, Lu Y (2011) single-crystal-like titania mesocages. *Angew Chem Int Ed* 123:1137–1140. doi:10.1002/ange.201004972

Blondeau M, Coradin T (2012) Living materials from sol-gel chemistry: current challenges and perspectives. *J Mater Chem* 22:22335–22343. doi:10.1039/c2jm33647b

Chen Y, Chang Y, Huang J, Chen I, Kuo C (2012) Light scattering and enhanced photoactivities of electrospun titania nanofibers. *J Phys Chem C* 116:3857–3865. doi:10.1021/jp2117246

Choi H, Antoniou M, Pelaez M, Delacruz A, Shoemaker J, Dionysiou D (2007) Mesoporous nitrogen-doped TiO₂ for the photocatalytic destruction of the cyanobacterial toxin microcystin-LR under visible light irradiation. *Environ Sci Technol* 41:7530–7535. doi:10.1021/es0709122

Cong Y, Zhang J, Chen F, Anpo M, He D (2007) Photocatalytic activity, and mechanism of nano-TiO₂ co-doped with nitrogen and iron. *J Phys Chem C* 111:10618–10623. doi:10.1021/jp0727493

Docampo P, Guldin S, Steiner U, Snaith H (2013) Charge transport limitations in self-assembled TiO₂ photoanodes for dye-sensitized solar cells. *J Phys Chem Lett* 4:698–703. doi:10.1021/jz400084n

Gao Y, Bai T (2013) Heat capacity for the binary system of quercetin + poly (ethylene glycol) 6000. *J Chem Eng Data* 58:1122–1132. doi:10.1021/je301114z

Goswami P, Ganguli J (2012) Evaluating the potential of a new titania precursor for the synthesis of mesoporous Fe-doped titania with enhanced photocatalytic activity. *Mater Res Bull* 47:2077–2084. doi:10.1016/j.materresbull.2012.03.037

Halasi G, Schubert G, Solymosi F (2012) Comparative study on the photocatalytic decomposition of methanol on TiO₂ modified by N and promoted by metals. *J Catal* 294:199–206. doi:10.1016/j.jcat.2012.07.020

Hao H, Zhang J (2009) The study of iron (III) and nitrogen co-doped mesoporous TiO₂ photocatalysts: synthesis, characterization and activity. *Microporous Mesoporous Mater* 121:52–57. doi:10.1016/j.micromeso.2009.01.002

Hartmann P, Lee D, Smarsly B, Janek J (2010) Mesoporous TiO₂: comparison of classical sol-gel and nanoparticle based photoelectrodes for the water splitting reaction. *ACS Nano* 4:3147–3154. doi:10.1021/nn1004765

Hu S, Wang A, Li X, Lowe H (2010) Hydrothermal synthesis of well-dispersed ultrafine N-doped TiO₂ nanoparticles with enhanced photocatalytic activity under visible light. *J Phys Chem Solids* 71:156–162. doi:10.1016/j.jpms.2009.10.012

Huang C, Yang Y, Doong R (2012) Microwave-assisted hydrothermal synthesis of mesoporous anatase TiO₂ via sol-gel process for dye-sensitized solar cells. *Microporous Mesoporous Mater* 142:473–480. doi:10.1016/j.micromeso.2010.12.038

Huang T, Mao S, Yu J, Wen Z, Lu G, Chen J (2013) Effects of N and F doping on structure and photocatalytic properties of anatase TiO₂ nanoparticles. *RSC Adv* 3:16657–16664. doi:10.1039/c3ra42600a

Hung I, Wang Y, Huang C, Fan Y, Han Y, Peng H (2010) Effects of templating surfactant concentrations on the

- mesostructure of ordered mesoporous anatase TiO₂ by an evaporation-induced self-assembly method. *J Eur Ceram Soc* 30:2065–2072. doi:[10.1016/j.jeurceramsoc.2010.04.015](https://doi.org/10.1016/j.jeurceramsoc.2010.04.015)
- Jing D, Zhang Y, Guo L (2005) Study on the synthesis of Ni doped mesoporous TiO₂ and its photocatalytic activity for hydrogen evolution in aqueous methanol solution. *Chem Phys Lett* 415:74–78. doi:[10.1016/j.cplett.2005.08.080](https://doi.org/10.1016/j.cplett.2005.08.080)
- Kumaresan L, Prabhu A, Palanichamy M, Murugesan V (2011) Synthesis of mesoporous TiO₂ in aqueous alcoholic medium and evaluation of its photocatalytic activity. *Mater Chem Phys* 126:445–452. doi:[10.1016/j.matchemphys.2010.10.036](https://doi.org/10.1016/j.matchemphys.2010.10.036)
- Lee J, Orilall M, Warren S, Kamperman M, Disalvo F, Wiesner U (2008) Direct access to thermally stable and highly crystalline mesoporous transition-metal oxides with uniform pores. *Nat Mater* 7:222–228. doi:[10.1038/nmat2111](https://doi.org/10.1038/nmat2111)
- Li Y, Chen J, Liu J, Ma M, Li L (2010) Activated carbon supported TiO₂-photocatalysis doped with Fe ions for continuous treatment of dye wastewater in a dynamic reactor. *J Environ Sci* 22:1290–1296. doi:[10.1016/S1001-0742\(09\)60252-7](https://doi.org/10.1016/S1001-0742(09)60252-7)
- Liu X, Gao Y, Cao C, Luo H, Wang W (2010) Highly crystalline spindle-shaped mesoporous anatase titania particles: solution-phase synthesis, characterization, and photocatalytic properties. *Langmuir* 26:7671–7674. doi:[10.1021/la1009384](https://doi.org/10.1021/la1009384)
- Liu E, Guo X, Qin L, Shen G, Wang X (2012) Fabrication and photocatalytic activity of highly crystalline nitrogen doped mesoporous TiO₂. *Chin J Catal* 33:1665–1671. doi:[10.1016/S1872-2067\(11\)60437-3](https://doi.org/10.1016/S1872-2067(11)60437-3)
- Mangham A, Govind N, Bowden M, Shutthanandan V, Joly A, Menderson M, Chamber S (2011) Photochemical properties, composition, and structure in molecular beam epitaxy grown Fe “doped” and (Fe, N) codoped rutile TiO₂ (110). *J Phys Chem C* 115:15416–15424. doi:[10.1021/jp203061n](https://doi.org/10.1021/jp203061n)
- Rahim S, Ghamsari M, Radiman S (2012) Surface modification of titanium oxide nanocrystals with PEG. *Scientia Iranica* 9:948–953. doi:[10.1016/j.scient.2012.03.009](https://doi.org/10.1016/j.scient.2012.03.009)
- Rane K, Mhalsiker R, Yin S, Sato T, Cho K, Dunbar E, Biswas P (2006) Visible light-sensitive yellow TiO₂-xNx and Fe-N codoped Ti_{1-y}Fey O₂-xNx anatase photocatalysts. *J Solid State Chem* 179:3033–3044. doi:[10.1016/j.jssc.2006.05.033](https://doi.org/10.1016/j.jssc.2006.05.033)
- Silva C, Juárez R, Marino T, Molinari R, García H (2011) Influence of excitation wavelength (UV or visible light) on the photocatalytic activity of titania containing gold nanoparticles for the generation of hydrogen or oxygen from water. *J Am Chem Soc* 133:595–602. doi:[10.1021/ja1086358](https://doi.org/10.1021/ja1086358)
- Spadavecchia F, Ardizzone S, Cappelletti G, Oliva C, Cappelli S (2012) Time effects on the stability of the induced defects in TiO₂ nanoparticles doped by different nitrogen sources. *J Nanopart Res* 14:1301. doi:[10.1007/s11051-012-1301-y](https://doi.org/10.1007/s11051-012-1301-y)
- Su J, Zou X, Zou YC, Li G, Wang P, Chen J (2013) Porous titania with heavily self-doped Ti (3+) for specific sensing of CO at room temperature. *Inorg Chem* 52:5924–5930. doi:[10.1021/ic400109j](https://doi.org/10.1021/ic400109j)
- Wang X, Hu D, Yang J (2007) Synthesis of PAM/TiO₂ composite microspheres with hierarchical surface morphologies. *Chem Mater* 19:2610–2621. doi:[10.1021/cm062561g](https://doi.org/10.1021/cm062561g)
- Wang Y, Smarsly B, Djerdj I (2010) Niobium doped TiO₂ with mesoporosity and its application for lithium insertion. *Chem Mater* 22:6624–6631. doi:[10.1021/cm1020977](https://doi.org/10.1021/cm1020977)
- Wang J, Zhou Y, Hu Y, Ryan O, Shao Z (2011) Facile synthesis of nanocrystalline TiO₂ mesoporous microspheres for lithium-ion batteries. *J Phys Chem C* 115:2529–2536. doi:[10.1021/jp1087509](https://doi.org/10.1021/jp1087509)
- Wang D, Li X, Chen J, Tao X (2012a) Enhanced visible-light photo electro catalytic degradation of organic contaminants at iodine-doped titanium dioxide film electrode. *Ind Eng Chem Res* 51:218–224. doi:[10.1021/ie202009a](https://doi.org/10.1021/ie202009a)
- Wang P, Ao Y, Wang C, Hou J, Qian J (2012b) Enhanced photo electro catalytic activity for dye degradation by graphene-titania composite film electrodes. *J Hazard Mater* 223:79–83. doi:[10.1016/j.jhazmat.2012.04.050](https://doi.org/10.1016/j.jhazmat.2012.04.050)
- Wu Q, Krol RVD (2012) Selective photoreduction of nitric oxide to nitrogen by nanostructured TiO₂ photocatalysts: role of oxygen vacancies and iron dopant. *J Am Chem Soc* 134:9369–9375. doi:[10.1021/ja302246b](https://doi.org/10.1021/ja302246b)
- Wu Y, Xing M, Zhang J (2011) Gel-hydrothermal synthesis of carbon and boron co-doped TiO₂ and evaluating its photocatalytic activity. *J Hazard Mater* 192:368–373. doi:[10.1016/j.jhazmat.2011.05.037](https://doi.org/10.1016/j.jhazmat.2011.05.037)
- Xing M, Wu Y, Zhang J, Chen F (2010) Effect of synergy on the visible light activity of B, N and Fe co-doped TiO₂ for the degradation of MO. *Nanoscale* 2:1233–1239. doi:[10.1039/c0nr00078g](https://doi.org/10.1039/c0nr00078g)
- Yang M, Hume C, Lee S, Son Y, Lee J (2010) Correlation between photocatalytic efficacy and electronic band structure in hydrothermally grown TiO₂ nanoparticles. *J Phys Chem C* 114:15292–15297. doi:[10.1021/jp103764n](https://doi.org/10.1021/jp103764n)
- Yu J, Wang W, Cheng B, Su B (2009) Enhancement of photocatalytic activity of mesoporous TiO₂ powders by hydrothermal surface fluorination treatment. *J Phys Chem C* 113:6743–6750. doi:[10.1021/jp900136q](https://doi.org/10.1021/jp900136q)
- Yu S, Yun H, Lee D, Yi J (2012) Preparation and characterization of Fe-doped TiO₂ nanoparticles as a support for a high performance CO oxidation catalyst. *J Mater Chem* 22:12629–12635. doi:[10.1039/C2JM30360D](https://doi.org/10.1039/C2JM30360D)
- Zhang L, Zhu Y, He Y, Li W, Sun H (2003) Preparation and performances of mesoporous TiO₂ film photocatalyst supported on stainless steel. *Appl Catal B* 40:287–292. doi:[10.1016/S0926-3373\(02\)00154-6](https://doi.org/10.1016/S0926-3373(02)00154-6)
- Zhang R, Tu B, Zhao D (2010) Synthesis of highly stable and crystalline mesoporous anatase by using a simple surfactant sulfuric acid carbonization method. *Chem Eur J* 16:9977–9981. doi:[10.1002/chem.201001241](https://doi.org/10.1002/chem.201001241)
- Zhou M, Yu J, Cheng B, Yu H (2005) Preparation and photocatalytic activity of Fe-doped mesoporous titanium dioxide nanocrystalline photocatalysts. *Mater Chem Phys* 93:159–163. doi:[10.1016/j.matchemphys.2005.03.007](https://doi.org/10.1016/j.matchemphys.2005.03.007)
- Zhou C, Zhao X, Yang B, Zhang D, Li Z, Zhou K (2012) Effect of poly (ethylene glycol) on coarsening dynamics of titanium dioxide nanocrystallites in hydrothermal reaction and the application in dye sensitized solar cells. *J Colloid Interface Sci* 374:9–17. doi:[10.1016/j.jcis.2011.12.006](https://doi.org/10.1016/j.jcis.2011.12.006)
- Zhou G, Liu X, Nan C, Liu Y, Wang D, Chen X (2013) C/N-sensitized self-assembly of mesostructured TiO₂ nanospheres with significantly enhanced photocatalytic activity. *New J Chem* 37:2582–2588. doi:[10.1039/c3nj00003f](https://doi.org/10.1039/c3nj00003f)